UNIVERSITY OF TARTU
FACULTY OF SCIENCE AND TECHNOLOGY
INSTITUTE OF PHYSICS

ANATOLI VLADIMIROV

COMPARISON OF IMAGE QUALITY TEST METHODS IN COMPUTED RADIOGRAPHY

MSc thesis in
applied physics (medical physics)

Supervisor: KALLE KEPLER, PhD,
Head of Training Centre of Medical Physics and Biomedical Engineering

TARTU 2010

TABLE OF CONTENTS

ABBREVIATIONS

AAPM	American Association of Physicists in Medicine (USA)
AEC	automatic exposure control
ALARA	as low as reasonably achievable
BMTK	Training Centre of Medical Physics and Biomedical Engineering
CNR	contrast-to-noise ratio
CR	computed radiography
DDI	detector dose indicator
DICOM	Digital Imaging and Communications in Medicine (standard)
DQE	detective quantum efficiency
DR	digital radiography
ESF	edge spread function
FS	film-screen
IC	image criteria
ICRU	International Commission on Radiation Units and Measurements
IPEM	Institute of Physics and Engineering in Medicine (UK)
LSF	line spread function
MED	medical exposure directive (97/43/Euratom)
MTF	modulation transfer function
OD	optical density
PDF	probability distribution function
PMMA	polymethyl methacrylate
PSF	point spread function
PSP	photostimulable phosphor
QA	quality assurance
QC	quality control
QI	quality index
ROC	receiver operating characteristic
ROI	region of interest
SNR	signal-to-noise ratio
STUK	Finnish Radiation and Nuclear Safety Authority
TCDD	threshold contrast-detail detectability
VGA	visual grading analysis

1. INTRODUCTION

During past years most of radiographic departments in European Union have been successfully moved from film-screen (FS) based technology to filmless digital technology. The digital technology in diagnostic radiography in Estonia is mostly presented by semidigital computed radiography (CR) systems, with slowly increasing number of fully digital radiography (DR) systems [1]. The transition from a film-screen environment to a digital is not a simple matter. In this process, patient radiation doses could increase from 40 to 100 % [2]. However European directive (MED) 97/43/Euratom requires that medical exposures have to be justified and carried out in an optimized fashion [3]. The CR systems are much more tolerant of inappropriate technique because of high latitude of digital detectors and phosphor plates which makes possible systematic over-expose or unnecessary high doses with a good or even perfect image quality. With increasing awareness of the need for radiation protection, a paradigm shift can be observed from the principle of "image quality as good as possible" to "image quality as good as needed". However the image quality in medical imaging is a phenomenon of enormous complexity. It is extremely task dependent – the demands on noise level, resolution and contrast differing from discipline-to-discipline. It also involves many processes that are not fully understood and described, such as the effects of image processing and the anatomical background in an image on the signal detection and interpretation by the human observer. The problem also is that in digital radiography until now there is no certain approach how to keep constant image quality at different tube potentials in order to calibrate the automatic exposure control (AEC) and this makes urgent need to find out appropriate practical image quality test methods. At this moment different types of parameters for image quality optimisation have been proposed by medical physics researchers: detector entrance dose, pixel value, detector dose indicator (DDI), signal-to-noise ratio (SNR), contrast-to-noise ratio (CNR), threshold contrast-detail detectability (TCDD). The behaviour of CNR at different tube potentials was recently examined in Marshall study [4]. As result of that work the method of constant entrance surface dose for AEC calibration was proposed in order to keep same value of CNR. Unfortunately CNR does not give information on the perceptibility of details of different size, although it does provide data on how well objects of different attenuation can be imaged, the question is if that method is good enough for evaluation and maintenance of an adequate image quality. In the present work comparison of the suggested CNR method with alternative strategies have been presented for dose-quality

optimization, including introduction of the method by using physical measurements of threshold contrast-detail detectability (TCDD).

2. LITERATURE REVIEW

2.1 Developments in digital imaging

During many decades in 20th century conventional film-screen technology has been a gold standard for diagnostic imaging. Since its introduction almost 30 years ago, digital imaging is gradually replacing this well established technology. This is primarily due to the perceived advantages of radiation detection technology, digital image processing, archiving, optimisation of image acquisition and display independently. The wide dynamic range of digital system gives a great advantage in imaging of widely different attenuating structures [5, 6]. Nowadays computed radiography (CR) and digital radiography (DR) are digital technologies widely spread in most healthcare institutions. Concerning CR systems these use storage-phosphor image plates with separate image readout process which means an indirect conversion process; DR technology converts X-rays into electrical charges by means of a direct readout process using thin-film transistor (TFT) arrays. Depending on the type of X-ray conversion used, DR systems can be further divided into direct conversion with a flat-panel detector based on amorphous selenium (a-Se) and indirect conversion with a two stage technique based on scintillator such as caesium iodide (CsI) and a photodiode array of amorphous silicon (a-Si) [7].

Computed radiography was the first available digital technology for projected radiography, introduced in 1983 and future led to a commercial system from Fuji Photo Film (Tokyo, Japan) [8]. First DR flat-panel systems with integrated readout mechanisms were introduced in the market at the end of the 1990s [9]. DR flat-panel systems due to their higher detective quantum efficiency compared to CR have potential for dose reduction. In the same time CR systems have been seen as a cost effective and easily applicable route from film technology to digital imaging technology due to possibility of utilising the existing X-ray equipment [10]. At the present work only CR systems as most conventional digital imaging systems in the radiology departments in Estonia have been covered, whereas DR systems have remained out of the scope.

2.2. Image quality and radiation dose

Implementation of contemporary technology is a great challenge for a hospital medical physicist. European directive on usage of medical exposures 97/43/Euratom (MED) requires that medical exposures have to be justified and carried out in an optimized fashion. It emphasizes that EU member states shall adopt criteria of acceptability for radiological equipment in order to indicate when action is necessary, including, if appropriate, taking the equipment out of service [3,11]. A comprehensive, consistent suite of approaches to performance and safety assessment criteria of CR equipment has been proposed in the Report 91 by the UK Institute of Physics and Engineering in Medicine (IPEM) [12]. The IPEM Report 91 includes repeatability, uniformity, spatial resolution and threshold contrast detail detectability acceptability tests. The Report 93 of the Task Group 10 of the American Association of Physics in Medicine (AAPM) covers almost the same aspects but specifies more tests parameters and specifications for certain vendors such as Agfa, Fuji and Kodak [13]. International Commission on Radiation Units and Measurements (ICRU) has published special guidelines for assessment different aspects of image quality, including system noise analysis and receiver operating characteristic (ROC) analysis [14, 15].

Optimisation of medical imaging systems is necessary to fulfil the MED requirement of a good image quality at a radiation dose to the patient that is as low as reasonably achievable (ALARA principle) [16]. Because of relatively narrow latitude (dynamic range) of film-screen systems, the conventional film imaging gives no possibility to produce systematically too high patient doses due to image over-expose and film darkening. The CR systems are much more tolerant of inappropriate technique because of high latitude of digital detectors and phosphor plates which makes possible systematic over-expose or unnecessary high doses with a good or even perfect image quality. With increasing awareness of the need for radiation protection, a paradigm shift can be observed from the principle of “image quality as good as possible” to “image quality as good as needed.” The radiation dose to patients should follow the ALARA principle while still providing image quality adequate to enable an accurate diagnosis. ALARA does not necessarily mean the lowest radiation dose, nor, when implemented, does it result in the least desirable radiographic image quality. What, indeed, constitutes adequate image quality is still open for discussion for the various imaging tasks. Reduction of patient dose according to the ALARA principle is not only a question of selecting the right detector, but also requires the optimisation of the whole imaging chain and the selection of appropriate imaging parameters [17]. Patient dose is often described by the patient’s entrance surface dose, which is measured on the patient’s skin at the centre of the X-ray beam. An alternative

to this is to make the measurement free-in-air, without the contribution of the radiation that is backscattered from the patient, and to express the result in terms of air kerma. Organ doses and the effective dose cannot be measured directly in patients undergoing X-ray examinations, and these are difficult and time consuming to obtain by experimental measurements using physical phantoms. However, these can be calculated to a reasonable approximation, provided that sufficient data on the X-ray examination technique (including e.g. patient entrance dose value) are available. Today, such calculations are most often made using the Monte Carlo method, where random numbers are used for simulating the transport of radiation in a complex medium, in this case the human body. Since the first introduction in 1997 the researchers of the Radiation and Nuclear Safety Authority of Finland (STUK) have continuously developed the PCXMC program allowing computation of organ doses for patients of different ages and sizes in freely adjustable X-ray projections and other examination conditions that are used in projection radiography and fluoroscopy [18]. Although the methods and programs to assess patient dose are readily available, the different approaches and methods to assess clinical image quality are still developing [19]. The purposes of medical imaging are objectively well-defined, but it is very desirable to have quantitative methods of describing image quality. These methods are essential to the objective comparison of images and imaging systems, and the optimisation of imaging technique and system design. Optimisation is especially important to avoid an essential conflict between image quality and potential harm of the radiation dose to the patient.

The routine assessment and control of image quality, both technical and clinical, is a fundamental task associated with good practice. At present, in addition to subjective visual methods, there are available also automated methods that can be used to assess technical image quality associated with diagnostic imaging systems [20].

2.3. Image quality parameters

2.3.1. Objective image quality measurements

The automatic exposure control (AEC) for conventional film-screen systems was calibrated to give a similar optical densities (OD) independent from the range of tube potentials and thickness of patients. Variation in sensitivity of digital detectors and phosphor plates with X-ray photon energy is significantly different from that of screen-film systems. This requires the use of alternative parameters linked to image quality in DR and CR [21]. Performance of image quality is usually

evaluated by using objective physical characteristics of the imaging system such as spatial resolution, contrast, and noise [16]. Spatial resolution of a medical image describes the size of the smallest anatomical structures that can be represented independently in the image. The actual spatial resolution depends on the inherent contrast of an object and the sum of the blurring effects of all the elements in the imaging system including the imaged object itself. The interrelation between spatial resolution, contrast and noise is illustrated in Figure 2.1. [22].

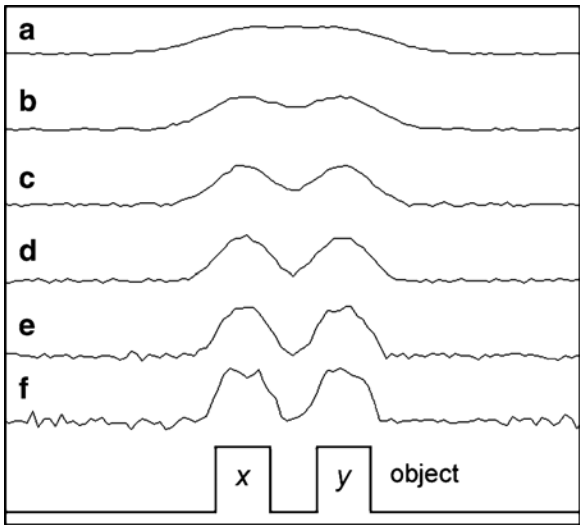

Figure 2.1. Relationship between spatial resolution, noise, and contrast. Profiles a–f represent images of a simple object that emits energy from two spatially distinct regions x and y. The spatial resolution increases progressively from a to f but the total signal, remains constant. Contrast, the difference in measured signal intensity from regions x and y relative to the background, increases with spatial resolution but so too does the noise level [22].

The choice of imaging method for a particular examination depends on the size of relevant anatomical features (spatial resolution required), the specificity of information required (the type of contrast). Contrast is a measure of the magnitude of the measured signal differences between physically different regions of the imaged object. When these measured signals are converted into an image 'contrast', it describes the magnitude of intensity differences between regions in the image. The signal contrast depends on the energy source and the physical properties of the imaged object – it describes the range of energies emitted by the object. The detector contrast depends on the way the signal emitted by the imaged object is modified (e.g. with a scatter suppression grid), detected, and recorded. The both signal and detector contrast form image contrast. In digital imaging it is very easy to enhance or reduce image intensity differences in order to make them more or less obvious to a human observer. This is the process of contrast adjustment. However, there is no way to enhance contrast if there is no difference in the measured signal or raw data. Also, a simple

contrast adjustment that amplifies recorded signal differences will also amplify any noise. The result may be no improvement in the ability to extract information from the image.

In general, contrast describes the intensity difference relative to the background:

$$C = \frac{I_0 - I_{bg}}{I_{bg}} \tag{2.1}$$

where I_o and I_{bg} are the average pixel intensities in the object and its background. No imaging method works without contrast and no imaging method is free of noise. If contrast is low and noise is high then the random intensity variations due to noise will make it difficult to visually detect the intensity changes due to contrast. Figure 2.2. illustrates how an increasing level of noise relative to contrast diminishes the ability to distinguish objects in an image.

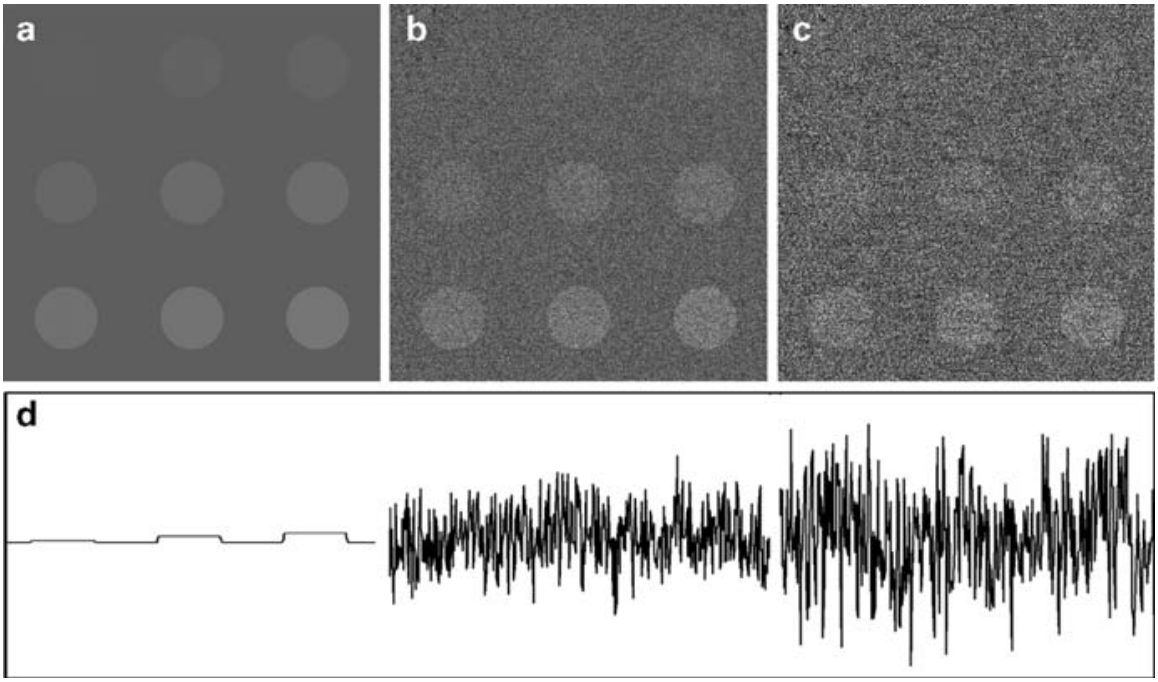

Figure 2.2. The presence of noise reduces our ability to extract information from an image. The noise-free test pattern (a) contains nine circles of equal diameter with contrast ranging from 0.003 to 0.069 In the presence of noise (images b and c) the visibility of the lower contrast objects is reduced or completely lost. Plot d shows the intensity profile through the top row of circles [22].

Noise interposes a random component into the image, and there are several sources of noise in an image (e.g. quantum noise, electronic noise, anatomic noise). The electronic noise comes from hardware associated with signal detection, amplification, recording and also by influence of electromagnetic radiation from external sources. The anatomical noise is given by the overlaying of structures within the patient resulting in image components that cannot be distinguished and therefore recognised as structures or some part of the scatter caused by the patient. The quantum

noise is an example of ‘measurement noise’ that is an inevitable consequence of the use of electromagnetic radiation as the imaging energy source. Quantum noise is the result of a Poisson process, meaning that if the standard deviation (σ) in the signal for all identical detector regions (pixels) is measured it will be equal to the square root of the average signal. The quantum noise decreases, relative to total intensity, with increasing measurement duration or signal energy flux. Random noise that enters the imaging system from external sources typically has a Gaussian, or normal, distribution. Noise can be characterized by a probability density function (PDF) – a summary of the statistical error due to noise in a recorded signal. Most image noise can be described by a Gaussian PDF (bell curve) with a characteristic standard deviation (σ) and sample mean (μ):

$$G(x) = \frac{1}{\delta\sqrt{2\pi}} e^{-\frac{(x-\mu)^2}{2\delta^2}} \qquad (2.2)$$

A Gaussian PDF means that 66% of all image pixels have an intensity error due to noise that is less than σ. A noisy image will have a larger value of σ [23]. In general, the Poisson distribution is exceedingly similar (not identical) to the Gaussian distribution when σ is set such that $\delta = \sqrt{\mu}$ Indeed, the Gaussian equation is often used to approximate the Poisson distribution with the above stipulation. [24].

An ideal image has high contrast, high spatial resolution, and low noise, however, these are not independent factors – these affect each other in complex and confusing ways. If either contrast or spatial resolution is too low, or if noise is too high then, as illustrated in Figure 2.3., the image is of no value – no clinical information can be extracted.

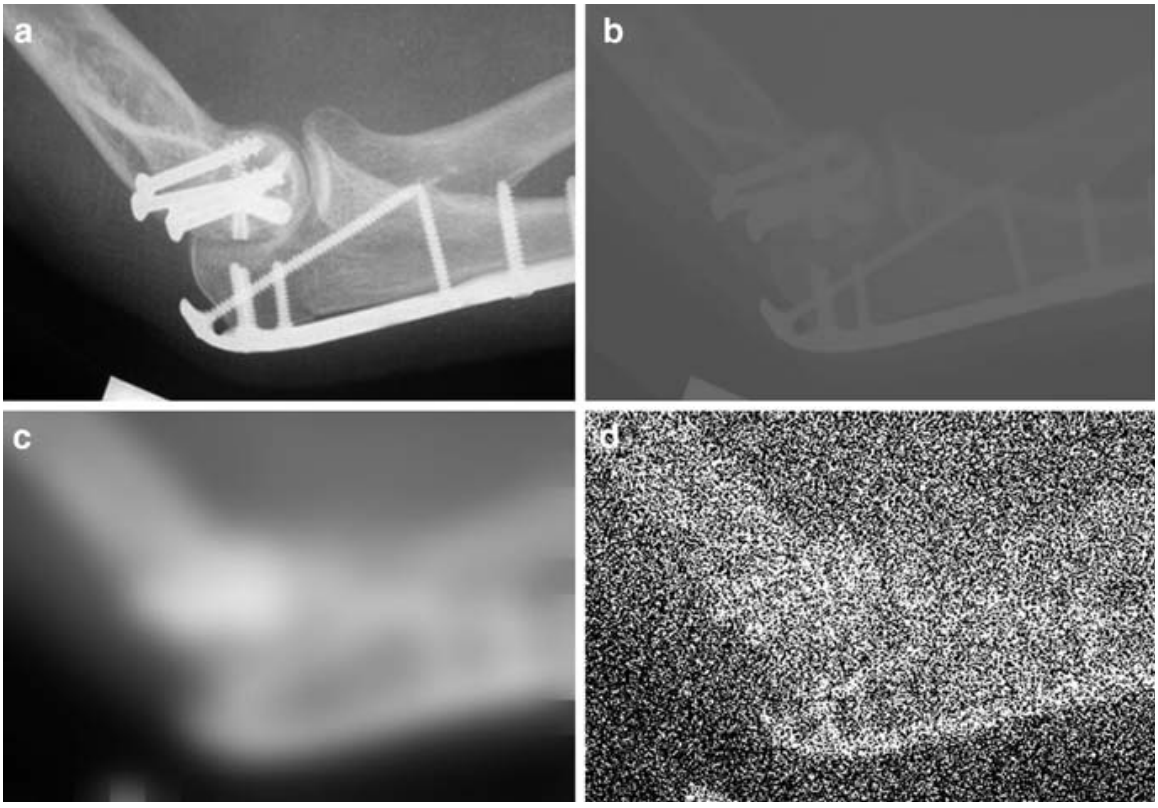

Figure 2.3. A useful image must have adequate contrast and resolution, and a low noise level, as illustrated in the image (a). Image b has high spatial resolution and low noise, but is rendered useless by having almost zero contrast. Image c has low noise and high contrast, but extremely poor spatial resolution. In image d we see high spatial resolution but the very high noise level has destroyed the contrast information [22].

The actual levels of needed contrast and resolution, and acceptable noise, depend on the purpose of the image. These also depend on innate properties of the object imaged (mostly tissue), the properties of the imaging system (hardware), and the way the system is used (technique). There are also other quality related secondary features, e.g. image uniformity, image aspect ratio and artefacts, which can be usually evaluated by test phantom images as a part of quality control (QC) [22, 25]. Because digital radiography systems have broader dynamic ranges than film and since the grey levels in the displayed digital image can be adjusted, the image quality is not so much contrast limited. As a result, it is the amount of noise in the image which limits the perception of detail and so the image quality, for most digital radiography systems. A common way to quantify the level of noise in an image is to estimate the signal-to-noise ratio (SNR) – the ratio of the mean signal of the object (the difference between the average pixel value in the object and the average pixel value in the background) and the pixel standard deviation in the background. [26]. Here it should be noted that the signal in the detector element is proportional to the number of photons imparting on it. Therefore signal-to-noise ratio (SNR) and thereby image quality is improved with higher exposure levels [27]. The energy detected by an imaging system can be thought of as being either signal

(contains information about the imaged object), or noise (contains no information and obscures the signal). SNR is a measure of the quality, or potential information content, of the image data. If the noise energy is random then SNR can be increased by increasing the total amount of energy measured – either by applying a more intense flow of energy, or by measurement over a longer time period. However validity of this measure of image quality is very limited. Although frequently used for objects of different size, the pixel SNR or SNR_p is the special case when the ideal observer's Rose model is applied to an object with a size given by one pixel [28].The Rose model is an attempt to describe how the human observer detects a flat-topped sharpedged signal of area A in a uniform background containing uncorrelated Poisson noise:

$$SNR_{Rose} = \frac{\langle \Delta n_s \rangle}{\langle n_b \rangle} \sqrt{A \langle n_b \rangle} \tag{2.3}$$

where the count level in the background is n_b expected number of photons per unit area, whereas the signal contains n_s extra photons per unit area.

The SNR_p is related to an observer that decides whether a signal is present or not by looking at the deviation of a single pixel value in the object from the pixel-to-pixel fluctuations in the background, without taking into account the size of the object, the size of the pixels or the texture of the noise. Such an observer has very little in common with the human observer. Consequently, the validity of using SNR_p as a meaningful measure of image quality is in general very low and its use should be avoided in the comparison of different imaging systems or different image processing techniques. However, as the reliability of the measure in general is high, it may be suitable for, for example, constancy control [29].

Another general problem with image SNR estimates is that these reveal nothing about the effect of noise on our ability to see objects in an image because visibility depends on contrast – the difference between signals. A highly overexposed radiograph might have a very high SNR and yet contain no useful information about the imaged object. A more useful estimate of the effect of noise on image information is the contrast-to-noise ratio (CNR):

$$CNR = \frac{\mu_A - \mu_B}{\sigma_{BG}} \tag{2.4}$$

In this expression noise is measured as the standard deviation of the background and the contrast measure is simply the intensity difference (μ_A- μ_B) between an object and its background.

The ability of visual detection of an object in an image depends not just on the CNR but also on the size of the object. Figure 2.2 shows a series of various size circles of constant CNR relative to the background. The largest circle is easy to see but the smallest, at the top left is effectively invisible.

Because our perception performs a local averaging of intensities larger objects are generally easier to see than smaller ones. The visibility of an object is roughly proportional to its area. It should now be clear that contrast, noise levels, and object size and shape all affect our ability to extract visual information from an image. There are several ways of measuring SNR and CNR and it is essential to specify the method used. The spatial resolution of an image is dependent on the construction and geometry of the imaging system, and the interaction of the imaging energy with the imaged object. All imaging systems blur the signal from the imaged object, and the object itself may scatter some of the imaging energy. The amount of blur is characterized by the point spread function (PSF) or the modulation transfer function (MTF). The PSF represents the image of a single (infinitely small) point in an imaged object. The MTF is the normalized (maximum scaled to 1.0) Fourier spectrum of the PSF. The MTF describes the progressive loss of image contrast due to blurring as spatial frequency increases. Both PSF and MTF may be difficult to measure directly in an imaging system due to the difficulty of producing suitable test objects. An approximation to the PSF can be derived from images of lines or edges which give, respectively, the line spread function (LSF) and edge spread function (ESF). Once the LSF is measured, the MTF can be computed directly from it using the fourier transform (FT):

$$\mathrm{MTF(f)} = |\mathrm{FT\{LSF(x)\}}| \tag{2.5}$$

There is also possibility incorporate all above mentioned parameters by using detective quantum efficiency (DQE) which describes the efficiency of an imaging system in the sense that it describes to what extent it utilises the information given as input to it. That the DQE takes both the sensitivity and resolution properties of an imaging system into account in the following way:

$$DQE(u,v) = \frac{MTF(u,v)^2}{NNPS(u,v)SNR_{in}^2} \tag{2.6}$$

where u and v denote orthogonal spatial frequencies for a two-dimensional imaging system, the MTF is the modulation transfer function of the system, describing to what extent the amplitude of a given spatial frequency passing through the system is preserved, and the NNPS is the normalized noise power spectrum, which describes the variance of image intensity spread over the spatial frequencies in the image. In the DQE computation, it is necessary to correct for the gain of the system, and the NPS given in units of digital value squared times mm^2 is divided by the square of

the mean value of the pixels used for analysis in units of digital value. This ratio is referred to as the normalized noise power spectrum (NNPS):

$$NNPS\ (u,v) = NPS\ (u,v) / (\text{large area signal})^2 \qquad (2.7)$$

It should be noted that in the literature, the terms “NPS” and “NNPS” are often used interchangeably to refer to the normalized noise power spectrum [30].

From the preceding discussion it should be clear that our ability to extract information from an image is primarily dependent on the image contrast, while the spatial scale of the information available is dependent on the spatial resolution of the image. Noise reduces our ability to detect subtle contrast differences. Noise has a much less significant effect on spatial resolution due to the tendency of our perception to perform a spatial averaging of intensities.

2.3.2. Observer performance methods

Observer performance methods could be grouped in two categories: observer performance methods based on lesion detection and methods based on visibility of anatomical structures. Both methods are used to evaluate the whole imaging chain and give a measure of the clinical image quality of an imaging system. The first category includes the methods used to detect lesions either in real patients or in phantoms: receiver operating characteristic (ROC) analysis and ROC related methods, such as free-response ROC (FROC), alternative free-response ROC (AFROC) and free-response forced error (FRE). ROC analysis offers several advantages as a measure of the accuracy of diagnostic tests:

a) it includes all possible cut points,

b) it shows the relationship between the sensitivity of a test and its specificity,

c) it is not affected by the prevalence of disease,

d) from it we can compute several useful summary measures of test accuracy (e.g. ROC curve area, partial area).

ROC analysis provides the most comprehensive description of diagnostic accuracy available to date [25, 29].

The second category includes the methods used to evaluate the visibility of anatomic structures such a visual grading analysis (VGA) and image criteria (IC). In VGA analysis, the aim is to compare the visibility of defined structures in a reference image. This evaluation is often based on a 5-level

grading scale for image comparison [31]. In IC analysis, the aim is to decide if the image criterion – based on a reference frame – is present or not in the image giving a score for that purpose. The criteria can be used to highlight optimum radiographic technique in terms of image quality and patient dose [29].

2.4. CR imaging chain

CR systems are based on an imaging plate that is similar to the image intensifying screen of conventional film radiography. As opposed to the screens of film radiography, this storage phosphor imaging plate retains the information of the incident photons as a latent image which can later be retrieved by stimulation by a read-out laser. The image plate is coated on one side with a layer of photostimulable phosphor material (PSP), which consists of a thin layer of phosphor crystals embedded in a binder. The commonest phosphor material is $BaFX:Eu^{2+}$ with X representing bromine or iodine atoms. Exposure of the image plate to X-ray photons stimulates electrons within the phosphor layer and traps them in a meta-stable state. CR plates have different absorption edge characteristics to rare-earth screens owing to their different elemental compositions. In the diagnostic energy range $BaF(Br_{0.85}I_{0.15})$, which is used by Agfa photo-stimulable phosphor plate (Agfa, Peissenberg, Germany), has a k-edge at, ~37 keV, whilst Gd_2O_2S (used for rare earth film-screens) has a k-edge at, ~50 keV. It can be seen from Figure 2.4. that between these energies (37 keV to 50 keV) the attenuation performance of the photo-stimulable phosphor will be better relative to the FS than at other energies [5].

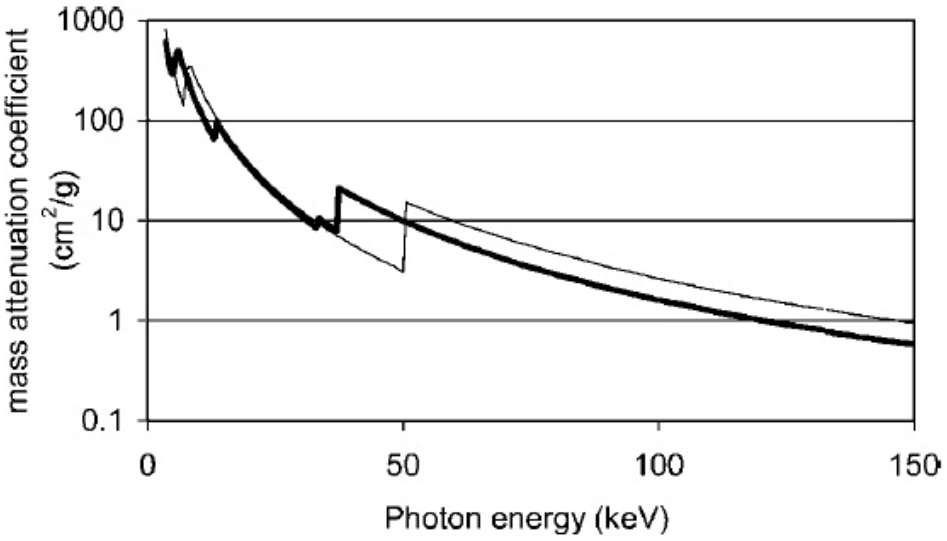

Figure 2.4. The mass attenuation coefficients of Gd_2O_2S (thin solid line) and $BaFB_{0.85}I_{0.15}$ (thick solid line) as a function of energy [5].

After exposure the cassette is inserted into the reader and this latent image of high-energy electrons can be read out by a thinly focused laser beam that releases the trapped electrons from their metastable state. When returning to their ground state, the electrons emit light which can be captured and the signal digitized. The amount of light is proportional to the intensity of the X-ray beam that had exposed the plate. The stimulated light emission is collected via a light guide, converted to electronic current by a photomultiplier, logarithmically amplified, filtered and finally digitized using a 12-bit or 16-bit analogue-to-digital converter. Following readout of the image plate, pre-processing automatically manipulates the data to optimise the display of the image, based on the examination or projection selected. This reduces the need for post-processing. Image processing critically influences image quality: automated windowing can provide optimum image density independent of exposure, adjustments of the gradation curves can simulate the characteristics of arbitrary film/screen systems, and frequency processing can enhance local contrast or even selectively enhance structures of a certain size or contrast.

The first versions of CR systems required more dose than screen film systems for similar clinical performance. However, already these systems allowed for flexible use of radiation dose with substantial dose reduction in situations where reduced image quality was acceptable. Detector material and read-out technology were continuously improved over the past years, which substantially improved dose efficiency and geometric resolution. With the most recent innovations, such as dual read-out technology or needle crystalline detectors, substantial improvements of dose efficiency became available. Dose efficiency is now approaching that of digital radiography systems and is better than that of a screen film combination with a speed class of 400 [6].

Automatic exposure control (AEC) devices are designed to improve the consistency of image acquisition in radiography. Such devices enable images to be recorded for patients of varying thickness, for different regions of the body, and with different tube potentials using exposures close to the optimum. This is achieved through automatic termination of exposures at preset air kerma levels at the image receptor. [32]. In general, AEC is accomplished by receiving a signal from sensor, integrating this signal in the appropriate control circuit and applying it to a comparator circuit. The reference side of the comparator is a voltage produced as a function of dose and selected tube potential. As the integrated signal reaches the reference level, a stop signal is produced to terminate the exposure. One of the problems with AEC has to do with the response of the sensors to changes in tube potential. In theory, the radiation at the paddle should be equal to the radiation presented to the cassette. However, as tube potential decreased, the quality of the beam also decreases, since potential affects the penetrating power of radiation. As tube potential is further

decreased, the quality of the radiation would be reduced to a point where the paddle would absorb more of the energy, thus leaving less energy to expose the cassette. When the paddle has been exposed to adequate radiation, the ramp to comparator would be sufficient to generate a stop signal. For film-screen technique, the radiation of the film is not adequate to achieve the desired film density, resulting in progressively lighter films as tube potential is decreased further. This problem is overcome using what is known as kV compensation, a method in which the selected tube potential is sensed and a signal is sent to the phototimer circuit to raise or lower its sensitivity, thereby compensating for variability by the paddle. Tube potential technique for digital systems is related to the fact that all digital detector mediums have – to a different extent, depending on their absorption characteristics – higher dose efficiency at lower tube potentials.

2.5. Different approaches to optimisation between image quality and exposure

Because of existence of fundamental differences between film-screen imaging and computed radiography (CR) the optimum AEC technique may not necessarily be the same [17].

CR image plates have different chemical composition than film and intensifying screens and consequently they have different energy response. Therefore, it is necessary to take into account the tube potential compensation curve tailored to the CR system rather than to use the existing film/screen curves.

It is generally the responsibility of the X-ray equipment supplier to set up the AEC on the X-ray system. However, the supplier of the CR system should provide sufficient information to allow optimal set-up of compensation curves and receptor doses. Failure to undertake this optimisation step can lead to over-exposure of the patients. Typically the manufacturer has calibrated the AEC system to the air kerma to demonstrate the best performance of detector without care of patient doses. Image quality is related to radiation exposure received by the detector. Although a relatively low exposure will result in a noisy image, it may still contain sufficient information to be diagnostically acceptable. A high exposure will result in improved image quality since quantum noise is reduced. However, image quality improvement is not linear, it will eventually level off as the quantum noise becomes less dominant and decrease as the plate becomes overexposed. Ideally, a system should be set up to obtain adequate image quality for the lowest possible dose [10]. There are several methods of AEC sensitivity calibration.

2.5.1. Detector dose indicator (DDI) based control

Doyle and Martin have calculated theoretical tube potential correction curves for CR detectors. The manufacturers of digital imaging systems use a variety of detector dose indices (DDIs) related to the amount of light generated from the phosphor, either by photo-stimulable luminescence in the case of computed radiography (CR). The DDI values are calculated from analysis of the histogram of image pixel values over an appropriate region of interest and provide a quantity that is related to the detector sensitivity. Images with a similar value for the DDI should have a consistent level of image quality at different tube potentials. Maintaining a constant DDI is recommended by Doyle as the method of choice for setting up AECs for digital radiography [32]. According to Doyle experiments the DDI, pixel value and SNR indicators demonstrate a similar trend within ±2% and should therefore have equal validity in determining the correct tube potential compensation curve Figure 2.5. The relationship between pixel value or DDI and exposure may not be linear and so must be measured and is known as the signal transfer property [12].

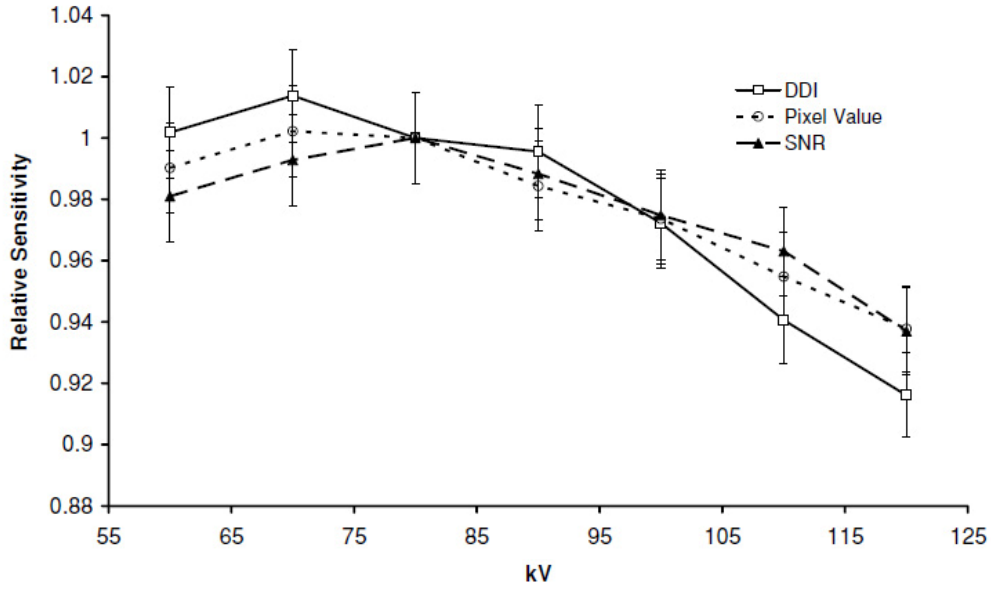

Figure 2.5. Comparison of the relative sensitivities of indicators that relate to image plate response for an Agfa CR system, normalized to the response at 80 kV. Error bars indicate an achievable tolerance of 3% in adjusting the AEC [26].

In this method acceptable noise level in images could be a main question for calibration of minimum required dose for AEC baseline.

2.5.2. Contrast-to-noise ratio (CNR) based control

AEC systems set up to hold air kerma constant or nearly constant at the X-ray detector will not maintain a constant level of contrast detail detectability as X-ray energy changes. The constant CNR method (also known as the signal difference to noise ratio (SDNR)) is more suitable maintaining constant detectability [4].

One of the earliest uses of the CNR in the optimization of signal detectability was given by Zamenhof (1982), who described an application in fluoroscopic imaging [33]. Now that digital imaging systems are in common use, there has been renewed interest in the CNR as a parameter for the image quality characterization and possible optimization of digital imaging systems [34, 35].

The CNR is often used to obtain practical measures of object detectability. The CNR concept is officially included in European Digital Mammography Protocol (EC 2006); however it does not insist the constant CNR for AEC performance [36]. The mammography protocol allows a 50% reduction in the CNR for AEC systems as the breast thickness changes from 2 cm to 9 cm. This will lead to some loss in contrast-detail detectability for larger breast sizes; however, allowing the CNR to fall for thicker breasts will reduce breast dose and allow shorter exposure times. According to Marshall experiments Figure 2.6. plots entrance surface dose (ESD) for the constant air kerma and constant CNR modes [4]. The ESD for constant air kerma at the CR cassettes shows the classical ESD response, where high tube potentials can be used to obtain low skin doses for a given examination (higher beam energy gives greater penetration through the phantom, leading to lower

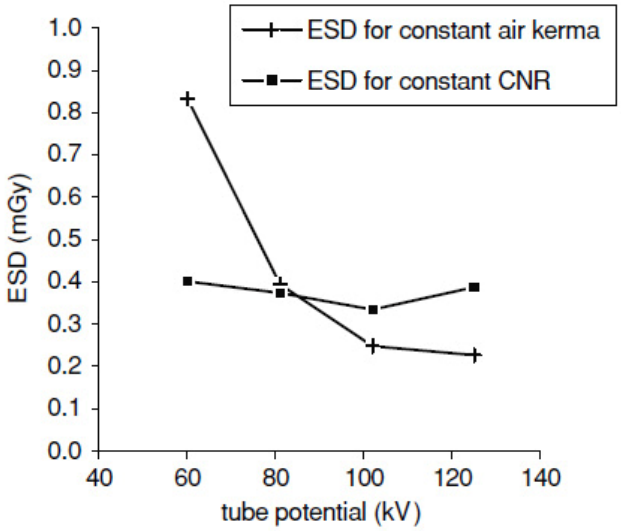

Figure 2.6. Entrance surface dose (ESD) measured at the input to the 20 cm tissue equivalent phantom for the constant air kerma at the CR cassette (~3 μGy) and for the constant target CNR method [4].

mAs values and hence a reduction in ESD is accompanied by a reduction in the number of discs seen (essentially a reduction in simple detectability). The results for the constant CNR show ESD to be approximately independent of tube potential, with no particular tube potential favoured for this detector.

The maximum deviation in ESD from the 81 kV figure is 11%, which occurs at 102 kV. These results imply that implementation of the constant CNR strategy for the CR system can result in constant (simple) contrast-detail detectability while holding the ESD burden to the patient constant. The magnitude of ESD is a reflection of the target CNR value chosen – a higher CNR would increase ESD at all tube potentials. The problem is that the CNR does not give information on the perceptibility of details of differing size, it does provide data on how well objects of different attenuation can be imaged and this relative performance supposes to show similar trends for objects of all sizes [35]. However a CNR values in the range of different details and at different exposure values were evaluated by Rompado [37]. The Figure 2.7. demonstrate the great variability of CNR measurement depending on object resolution.

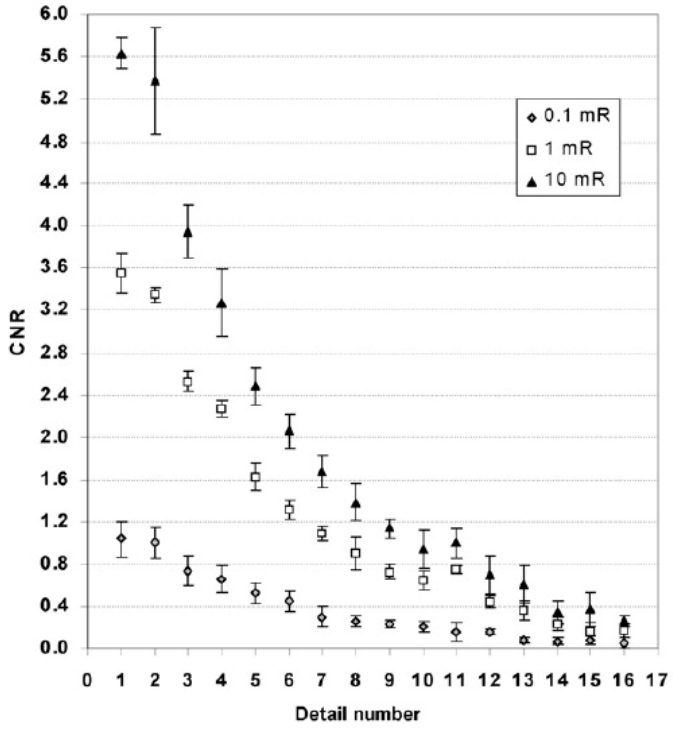

Figure 2.7. CNR values for different details of TOR (CDR) phantom and for three expose levels [37].

There are also some studies that show possibility to maximize CNR by optimise tube potential for different radiographic technique. Tube voltages that maximize the CNR for imaging the lung (60 kVp), heart/spine (80–125 kVp) and diaphragm (60–90 kVp) anatomical compartments have been suggested by Moore et al. [38].

2.5.3. Threshold contrast detail detectability (TCDD) based control

An alternative for assessment of physical image quality is the use of contrast detail test objects that provide a quantitative measure of image quality in terms of two fundamental parameters: low contrast and small detail detectability. Such methods involving test objects most frequently consider the overall imaging chain, including the human observer. Although these cannot be used to directly predict clinical image quality, due to the simplicity of the models used in comparison to the complexity of real anatomic structures, these provide useful information on threshold contrast-detail detectability (TCDD) and equipment performance. The use of contrast-detail images is a practical approach primarily adopted for routine quality control (QC) constancy testing [18].

For TCDD evaluation the CDRAD test objects (University of Nijmegen, Nederland) have been commonly used. These are used to derive the lowest contrast detectable (C_T) as a function of detail size. The CDRAD object consists of either a series of circular holes of different diameter and depth drilled into a tissue equivalent material (e.g. PMMA), or a series of circular objects positioned on a base material. Typically the number of details of each diameter visible in the image is recorded and used to calculate values of threshold contrast index,

$$H_T(A) = \frac{1}{C_T \cdot \sqrt{A}} \tag{2.8}$$

where A is the detail area and C_T is the minimum detectable contrast. C_T must be calculated for the specific beam conditions used (energy and filtration). The threshold contrast index data can be viewed graphically, or summarized as a single quality index (QI) [5, 39].

However, the subjective nature of human perception and the variations in the decision threshold pose limits to the minimum image quality variations detectable with reliability. Objective methods of assessment of image quality such as automated scoring overcome the above limitations [20, 40].

According to the previously published study the comparison of $H_T(A)$ curves could provide essential information on CR system response at different tube potentials and therefore to be used for optimisation of automatic expose control (AEC) of the system [41].

2.6. The aims of the thesis

The main aim of the thesis was to compare different strategies in dose-quality optimisation

The detailed goals of the conducted studies were:

- to carry out study of physical measurements of threshold contrast-detail detectability (TCDD) (H_T(A) index) at different tube potential values, with keeping constant detector entrance dose; surface entrance dose (ESD) and time-current product (MAS).
- to estimate uncertainty in measurement of threshold contrast-detail detectability (TCDD)
- to evaluate and compare image quality estimation methods for dose-quality optimisation in computed radiography (CR) systems.

3. MATERIALS AND METHODS

3.1 Imaging system

All test were performed in X-ray room equipped with overtable fluoroscopy system Iconos R100 Axiom (Siemens Medical Solutions, Erlangen, Germany) assembled with X-ray tube Optitop 150/40/80HC (tungsten target, anode angle 16°) and additional filtration of 0,1 mm Cu with total inherent filtration equivalent to 6,7 mm of aluminium (Al) and vertical bucky with moving antiscatter grid (focus distance 180 cm, 70 lines cm^{-1}, grid ratio 7:1). The measured output curve of the X-ray tube is given in Figure 3.1. Images were acquired with storage phosphor plates of type MD 4.0 (35 cm x 43 cm, effective pixel pitch of 0,167 mm) (Agfa Healthcare, Mortsel, Belgium) and the phosphor plates were scanned by Agfa CR-35X digitizer with software version Agfa NX 1.0 (build 1.0.3203).

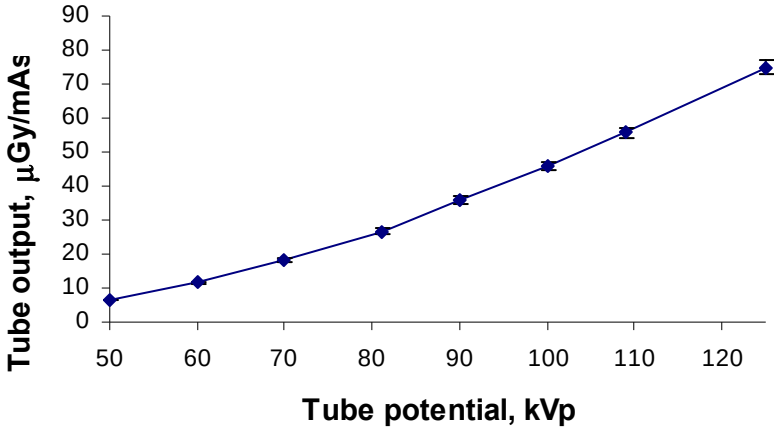

Figure 3.1. Radiation output Y versus tube potential KVp of the X-ray tube, measured at a distance of 100 cm from the focal spot (large focus of 1.0 mm, HVL = 4,6 mm Al @ 81 kV, values of Y are given with standard uncertainty bars and second order regression line).

3.2. Contrast-detail phantom

The threshold contrast-detail detectability was assessed using the CDRAD contrast-detail phantom (Artinis Medical Systems B.V., Zetten, The Netherlands). The CDRAD phantom consists of a 10 mm thick, 265 x 265 mm^2 wide polymethyl metacrylate (PMMA) support in which circular holes of

15 different diameters (ranging from 0,3 mm to 8 mm) have been drilled of 15 different depths (ranging from 0,3 mm to 8 mm) (see Figure 3.2).

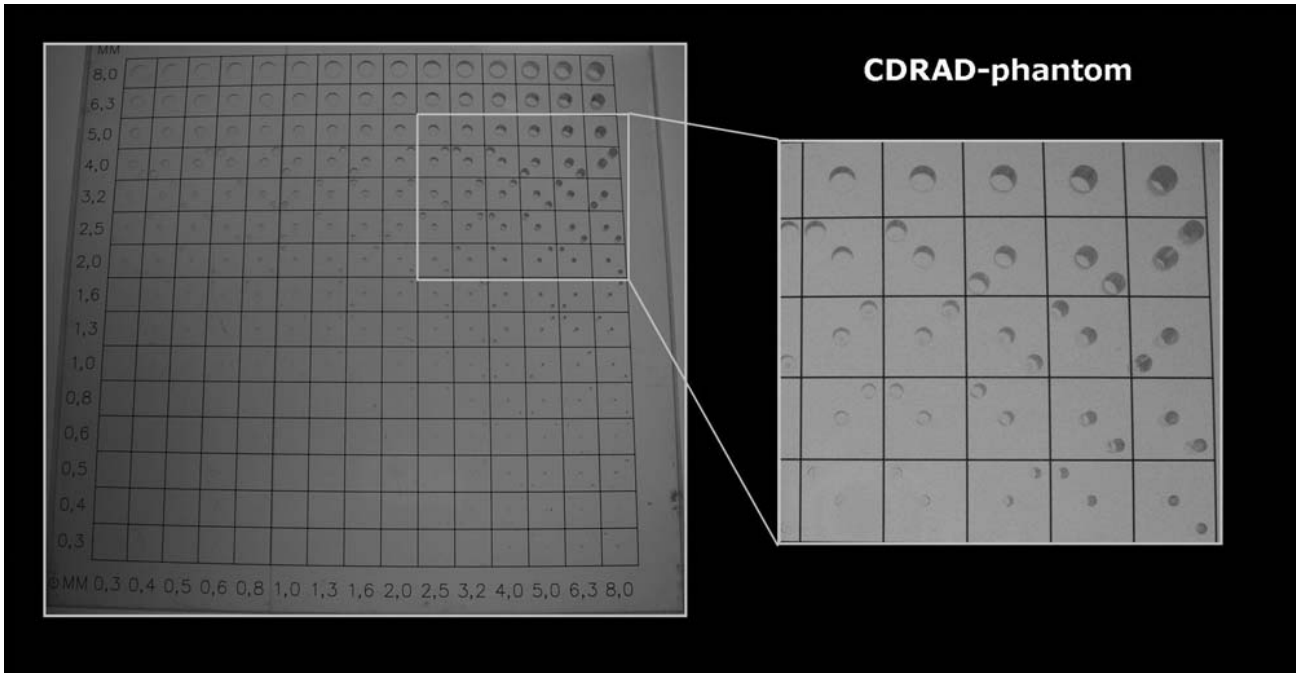

Figure 3.2. Picture of the CDRAD contrast-detail test object. This phantom is fabricated in PMMA and contains cylindrical holes of various diameter 0,3–8,0 mm and depth 0,3–8,0 mm.

The holes have been arranged in a 15 x 15 matrix. Rows contain holes of identical diameter and exponentially increasing depth. Columns contain holes of identical depth and exponentially decreasing diameter. Square matrix element of the first three rows contains one hole in the centre. Each square matrix element of the remaining 12 rows contains two identical holes; one in the centre and a second one randomly placed in one of the four corners. The detail depths are such that within a reasonable range of exposures some, but not all, of the details should be visible at all detail diameters. In this work the CDRAD phantom was placed between two 75 mm (3 × 25 mm) PMMA plates to provide scatter and give attenuation similar to an adult patient. This gives the total thickness of the CDRAD-PMMA phantom of 160 mm PMMA. All exposures were made in the vertical bucky stand with a moving antiscatter grid and a focal spot to detector distance of 200 cm in order to reduce parallax effect as much as possible. Large focal spot (1.0 mm) of the X-ray tube was selected. In order to have the X-ray beam collimated in the CDRAD-PMMA phantom area, the field size of 19 x 19 cm^2 (projected on the phosphor plate plane) was chosen on the collimator. The setup geometry is shown in Figure 3.3.

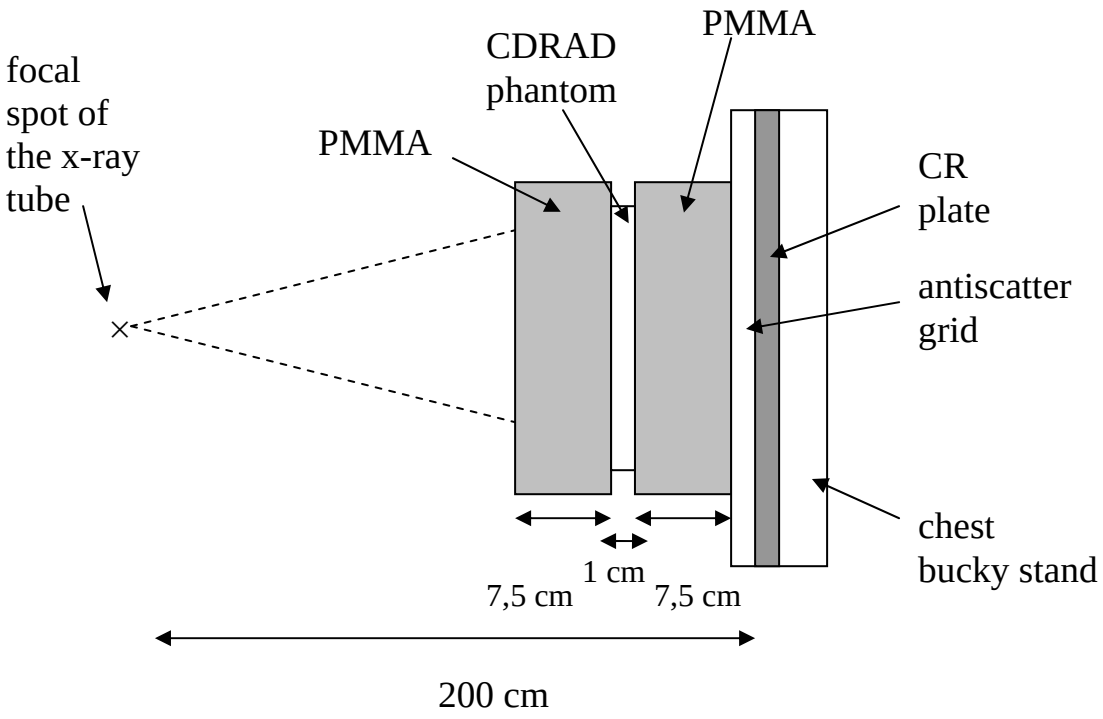

Figure 3.3. A schematic diagram of the experimental setup.

3.3. Detector constant entrance dose setup

At first stage of experiment the tube potential of 81 kVp and central sensor for AEC system was chosen, together with high speed sensitivity settings (speed class "H"). Detector entrance dose of 3,9 μGy was used as the reference to obtain images with same entrance dose at 60 kVp, 100 kVp and 125 kVp (Table 3.1.). Image receptor entrance dose with the phantom in place was measured with a Keithley TRIAD dosimeter and a 15 cm^3 ionization chamber (Keithley Instruments Inc., USA) placed directly inside the bucky cassette holder.

Table 3.1. Setup for constant detector dose measurements.

Tube potential, kVp	Tube charge, mAs	Detector entrance dose, μGy
60	110	3,8
81	28	3,9
100	11	3,8
125	5	3,8

Reference exposure at 81 kVp was repeated 10 times in order to estimate uncertainty in the measurements.

3.4. Phantom constant entrance dose setup

At second stage in order to keep constant CNR according to Marshall method the constant value of ESD about 0,38 mGy at phantom entrance surface was selected and set as the reference dose level for obtaining images at potentials of 60 kVp, 100 kVp and 125 kVp (Table 3.2.) [4]. Phantom entrance dose was measured with the same Keithley ionization chamber placed directly at the centre of CDRAD-PMMA phantom entrance plane.

Table 3.2. Setup of constant ESD measurements.

Tube potential, kVp	Tube charge, mAs	Phantom entrance surface dose, mGy	Detector entrance dose, µGy
60	65	0,38	2,3
81	28	0,39	3,9
100	16	0,37	4,9
125	10	0,39	6,3

At last stage the setup values of 81 kVp and 28 mAs were used as the reference to obtain images with same time-current product (MAS) at 60 kVp, 100 kVp and 125 kVp (Table 3.3.).

Table 3.3. Setup of constant MAS measurements.

Tube potential, kVp	Tube charge, mAs	Detector entrance dose, µGy
60	28	1,1
81	28	3,9
100	28	10,2
125	28	21,6

The CR plates were read out in Agfa CR-35X scanner without clinical post-processing by using the "system diagnostics" and "flat field" settings. The DICOM greyscale image window and level were adjusted manually such that the visibility of the details appeared to be maximized and the background noise remained perceptible.

The contrast of detail is defined as:

$$C = \frac{|I - I_D|}{I} \qquad (3.1)$$

where I is the primary transmission through the full phantom thickness of 160 mm and I_D is primary transmission through the contrasting detail of the CDRAD phantom and the PMMA phantom of 150 mm.

To estimate the detail contrast, the transmitted air kerma (the phantom output) was calculated for the particular CDRAD detail with the PMMA phantom at different tube potentials by using relevant tube data (tungsten target, anode angle 16°, ripple of the generator voltage 5 %) and spectral data derived from IPEM Report 78 [42]. An X-ray spectrum calculated for the reference potential of 81 kVp is given in Figure 3.4.

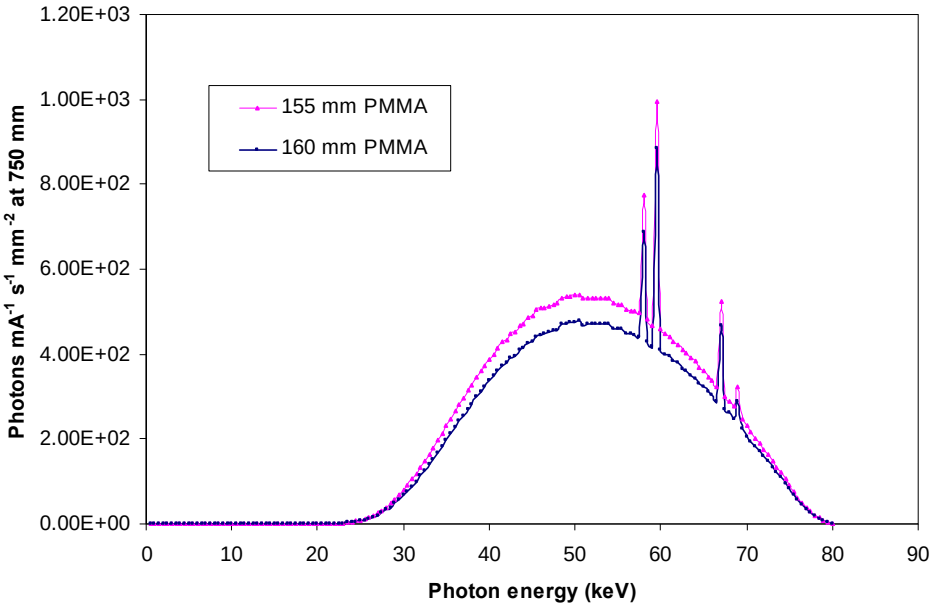

Figure 3.4. Calculated X-ray photon spectrum for 155 mm and 160 mm of PMMA (tube voltage 81 kVp, ripple 5 %, total filtration 4,4 mm Al, anode angle 16°, target material W).

The CDRAD phantom was used to measure the lowest contrast detectable (C_T) as a function of detail size. All CDRAD DICOM images were evaluated (including finding threshold contrast-detail curves) with CDRAD Analyzer software v1.1 (Artinis Medical Systems B.V., Zetten, The Netherlands) [40]. The pattern of the CDRAD 2.0 phantom and the radiographic DICOM image of the phantom (at 81 kVp, 15 cm PMMA) are given in (Figure 3.5.).

The lowest contrast detectable (the threshold contrast level) was determined by the computer analysis. Using the Student t-test with Welch correction the program determines if the contrast-detail combination in a certain square is positively seen. The same Alpha level of significance (Alpha=1e-008) was selected for all evaluations. This level set for automated software evaluation has a best correlation with a visual scoring by an average observer [20]. The contrast detail score diagram and the contrast detail curve of the evaluated CDRAD phantom DICOM image acquired at 81 kVp with 15 cm PMMA are shown in Figure 3.6.

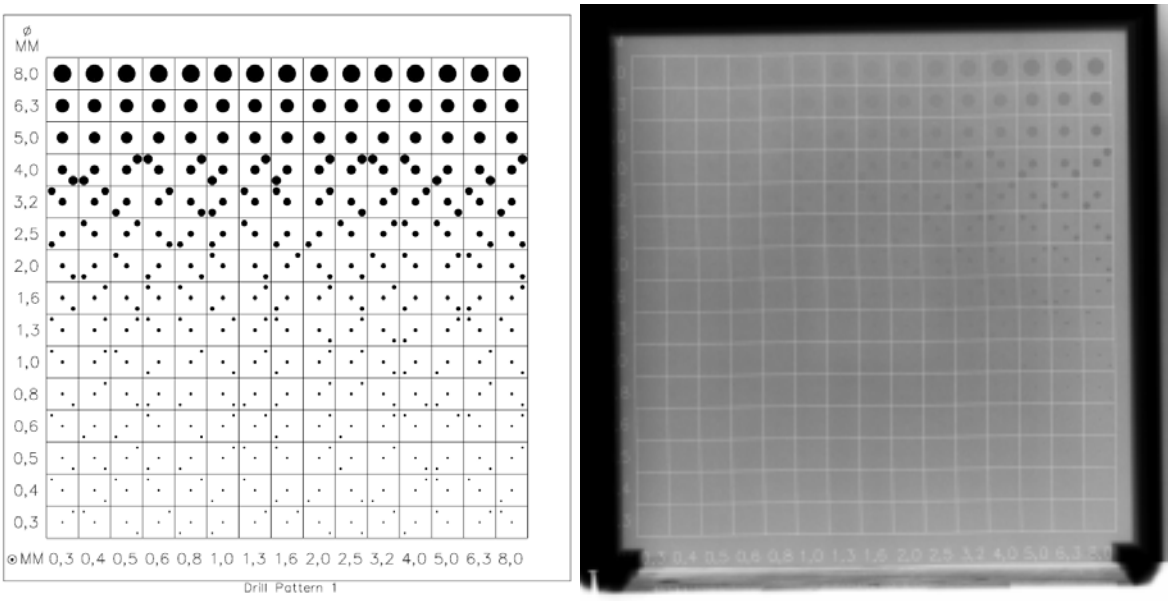

Figure 3.5. Pattern of the CDRAD 2.0 phantom and radiographic DICOM image of the CDRAD with 15 cm standard PMMA phantom.

The data were presented graphically as the TCDD index $H_T(A)$ against the square root of detail area A (in mm) by the formula [39]

$$H_T(A) = \frac{1}{C_T \cdot \sqrt{A}} \tag{3.2}$$

where C_T is the detected threshold contrast. It was also calculated the ideal $H_T(A)$ curve by using ideal conditions were CDRAD phantom holes fully visible and maximum lowest contrast detectable over every detail size.

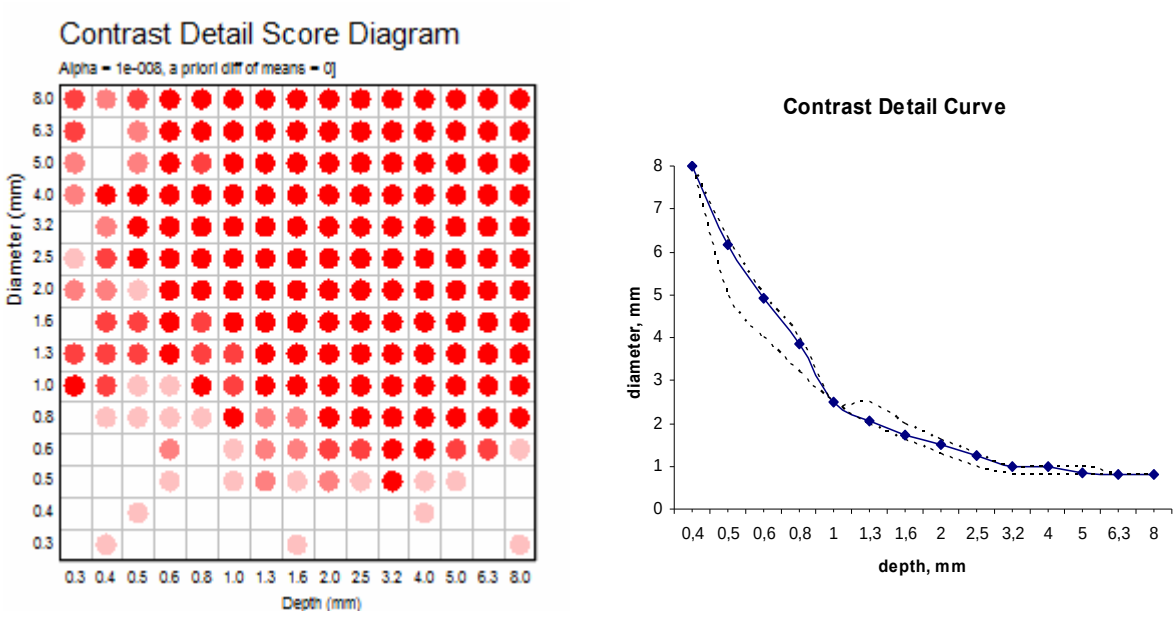

Figure 3.6. Contrast detail score diagram (left) and contrast detail curve (right) of mean value with a maximum and minimum deviations of ten measurements of the CDRAD phantom, DICOM image acquired at 81 kVp with 15 cm PMMA.

3.5. Uncertainty of measurements

Unaccuracy and uncertainty of measurements was estimated. During general quality control (QC) measurements of equipment it was found that maximum tube voltage unaccuracy is (2,7 ± 1,7) %.

In order to estimate the uncertainty in measurements of air kerma, detector entrance dose and TCDD (index $H_T(A)$) the exposures of CDRAD were repeated 10 times and the corresponding DICOM images were evaluated by the CDRAD Analyzer software.

Combined standard uncertainty was calculated by formula

$$u_C(K) = \sqrt{u_A(K)^2 + u_B(K)^2} \tag{3.3}$$

where u_A is the component of uncertainty arising from random effects (e.g. reproducibility of dose meters and reproducibility of X-ray output)

$$u_A(K) = s(\overline{K}) = \sqrt{\frac{\sum_{i=1}^{n}(K_i - \overline{K})^2}{n(n-1)}} \tag{3.4}$$

u_B is the component of uncertainty arising from systematic effects (e.g. accuracy of the dosimeter).

$$u_B(K) = \frac{1{,}65\delta(K)}{\sqrt{3}} \tag{3.5}$$

The expanded uncertainty U was calculated with coverage factor k = 2,26 (corresponding to a level of confidence of about 95%)

Uniformity of response is a fundamental parameter for detectors in all imaging fields. A uniform exposure should result in a uniform response of the CR system [37]. The uniformity was evaluated by measurement of average pixel values of 100 x 100 pixels region of interest (ROI) at centre and in four different quadrants of the reference image. In order to produce homogenous image the detector constant dose setup was used with 15 cm PMMA without CDRAD phantom (Table 3.4.).

Table 3.4. Uniformity of image at 81 kV and 15 cm PMMA with detector dose of 3,9 μGy

	Measured pixel value with ROI of 100x100 pixels	Deviation from central ROI, %
center	14691	0
left	14085	4,1
right	14113	3,9
up	14405	1,9
down	15262	3,8

4. RESULTS AND DISCUSSION

4.1. Threshold depth-diameter analysis

The aim of this work is to compare the different methods of AEC calibration through comparison of threshold contrast-detail index. The Figure 4.2. shows comparison of $H_T(A)$ index at different tube potentials with keeping constant detector entrance dose of 3,9 μGy. The ideal $H_T(A)$ curve also presented to demonstrate the best theoretically possible threshold contrast-detail detectability. It was calculated for the case when threshold contrast of 0,3 mm of the smallest possible hole depth was detectable at each diameter.

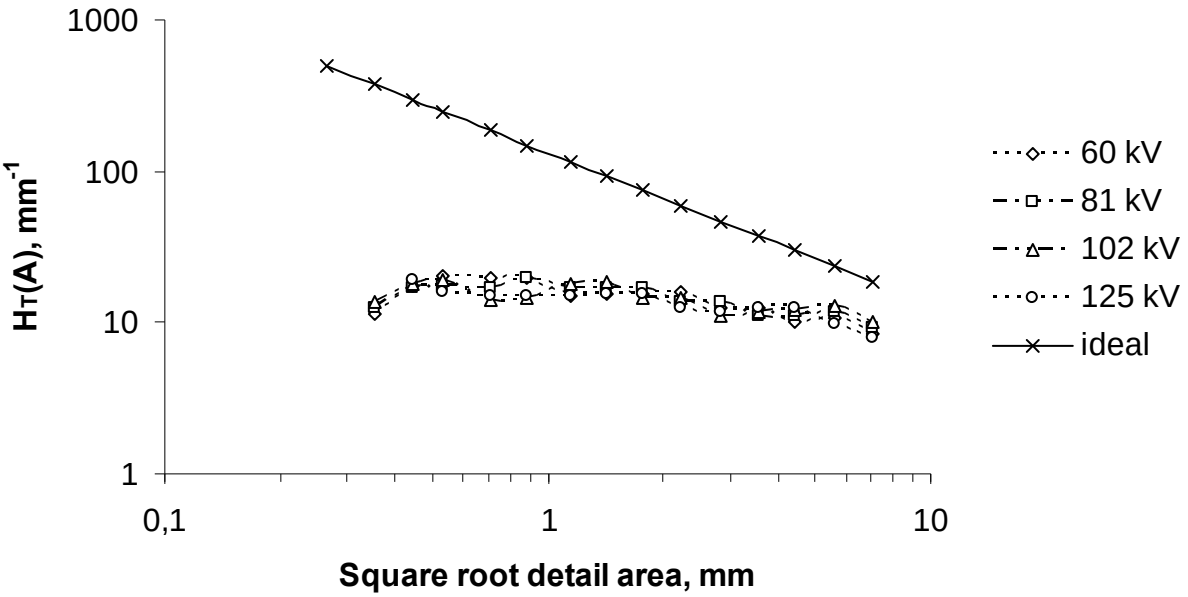

Figure 4.2. Comparison of the threshold contrast-detail index at different tube potentials by using same 3,9 μGy detector entrance dose (15 cm PMMA + CDRAD).

Standard deviations of the single measurements of each value of $H_T(A)$ index for 60 kVp, 100 kVp and 125 kVp from reference 81 kVp was calculated. The average standard deviation for constant detector entrance dose method was 1,7 mm^{-1}. The Figure 4.3. shows the comparison of threshold contrast-detail index at different tube potentials when using constant patient entrance dose or ESD which could be corresponded according to Marshall study to the constant contrast-to-noise ratio

(CNR) [4]. In order to do that the constant patient entrance dose ESD was kept around level of 0,39 mGy which corresponds to well optimised system according the previous studies [43].

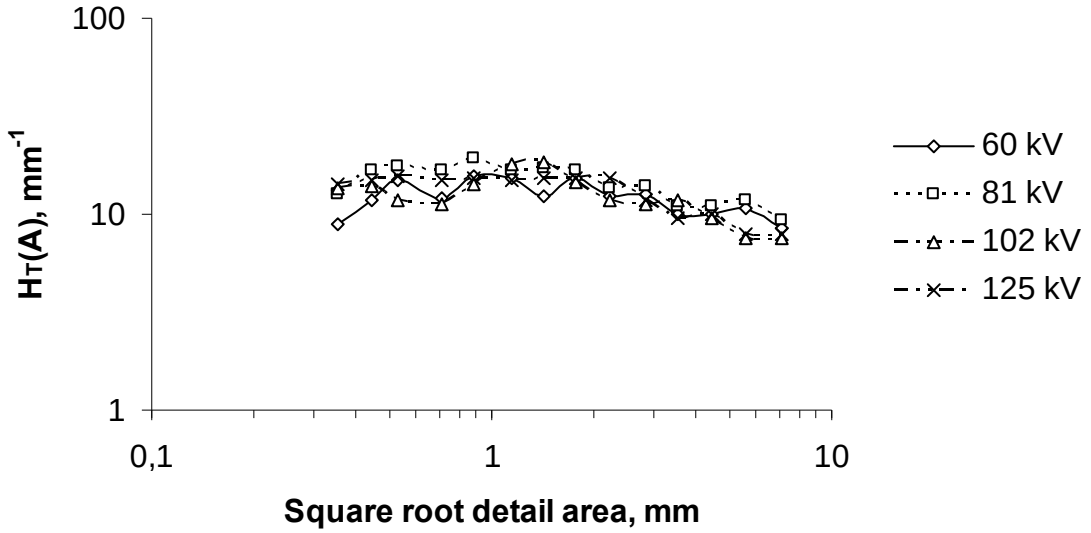

Figure 4.3. Comparison of the threshold contrast-detail index at different tube potentials using the same 0,39 mGy entrance surface dose (ESD) in order to keep constant CNR (15 cm PMMA + CDRAD).

For constant CNR method the average standard deviation of $H_T(A)$ index for 60 kVp, 100 kVp and 125 kVp from reference 81 kVp curve is 2,4 mm^{-1} which is 41% more compare to constant detector dose method. In the same time the average absolute value of $H_T(A)$ index is about 10% more for constant dose detector method.

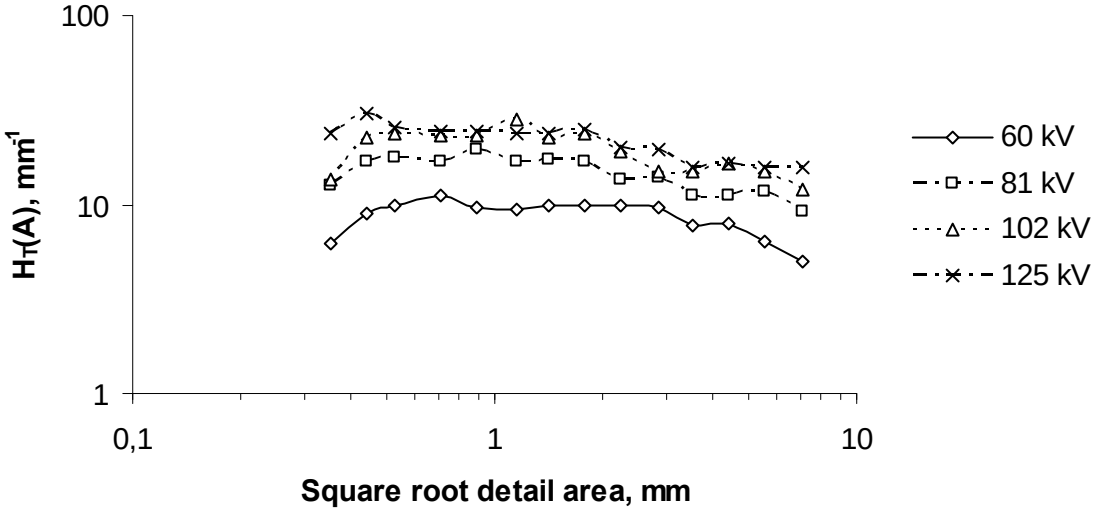

Figure 4.4. Comparison of the threshold contrast-detail index at different tube potentials using same time current product (28 mAs) (15 cm PMMA + CDRAD).

The Figure 4.4. shows the effect of tube potential to the contrast-detail index curve without any AEC calibration and by using constant time-current product. Because lower tube potentials produce lower tube output (Figure 3.1.) it is clear, that lower KV will produce significantly lower ESD when the MAS value is kept constant and as result the lower image quality as well.

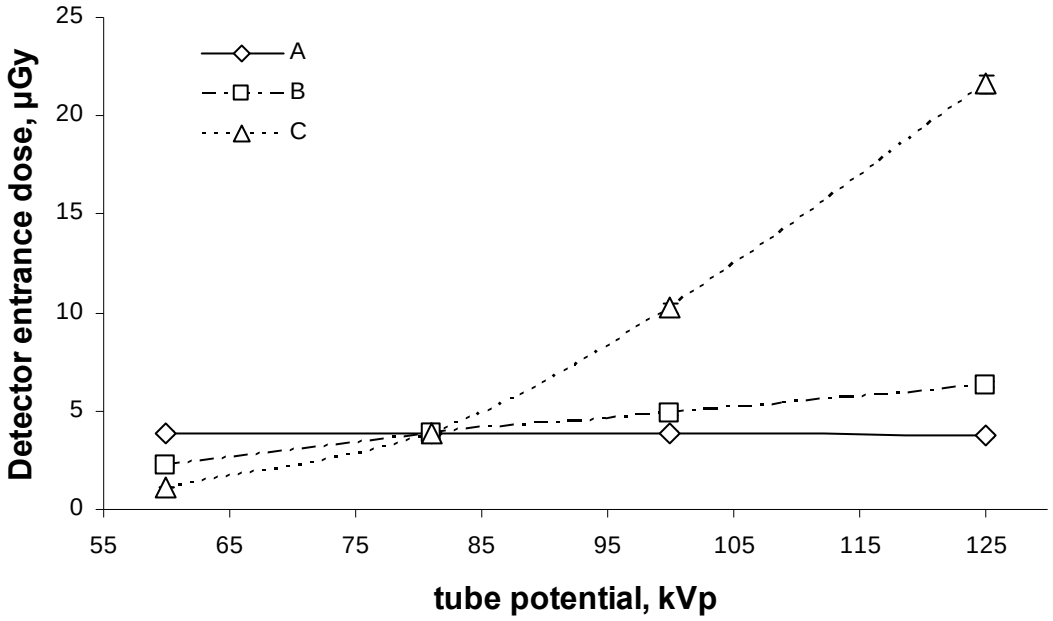

Figure 4.5. Comparison of detector entrance dose at different optimisation methods (15 cm PMMA + CDRAD): constant detector entrance dose (A); constant CNR (B); constant time-current product (MAS) (C).

The Figure 4.5. demonstrates how the AEC detectors could be practically calibrated in order to keep same detector entrance dose or ESD.

In Figure 4.6. the threshold contrast-detail index for two different methods is compared at 60 kVp. The average standard deviation of H_T(A) index at 60 kVp from reference 81 kVp curve is 1,5 mm^{-1} for constant dose detector method and 2,4 mm^{-1} for constant CNR method.

The Figure 4.6. shows that for 60 kVp at lower spatial frequencies or large details absolute value of H_T(A) index for the constant detector entrance dose method compared to the constant CNR method differs from 26% to 63%. In the same time at higher spatial frequencies (small details) the values of H_T(A) index are almost equal

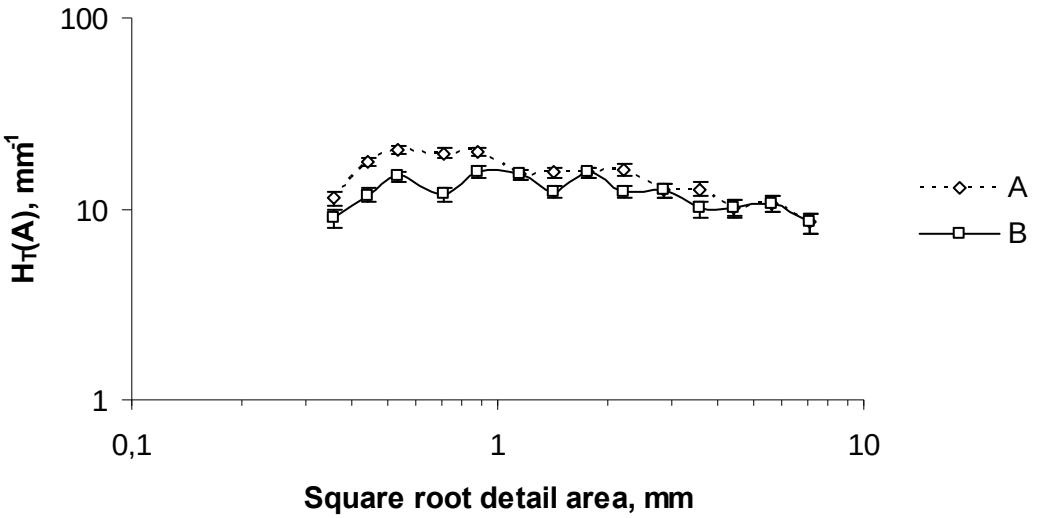

Figure 4.6. Comparison of the threshold contrast-detail index at 60 kVp with method based on constant detector entrance dose (A) and method based on constant CNR (B) (15 cm PMMA + CDRAD).

In the same way in Figure 4.7. the threshold contrast-detail index for two different methods is compared at 125 kVp. The average standard deviation of $H_T(A)$ index from reference 81 kV curve is 1,9 mm^{-1} for constant dose detector method and 2,0 mm^{-1} for constant CNR method.

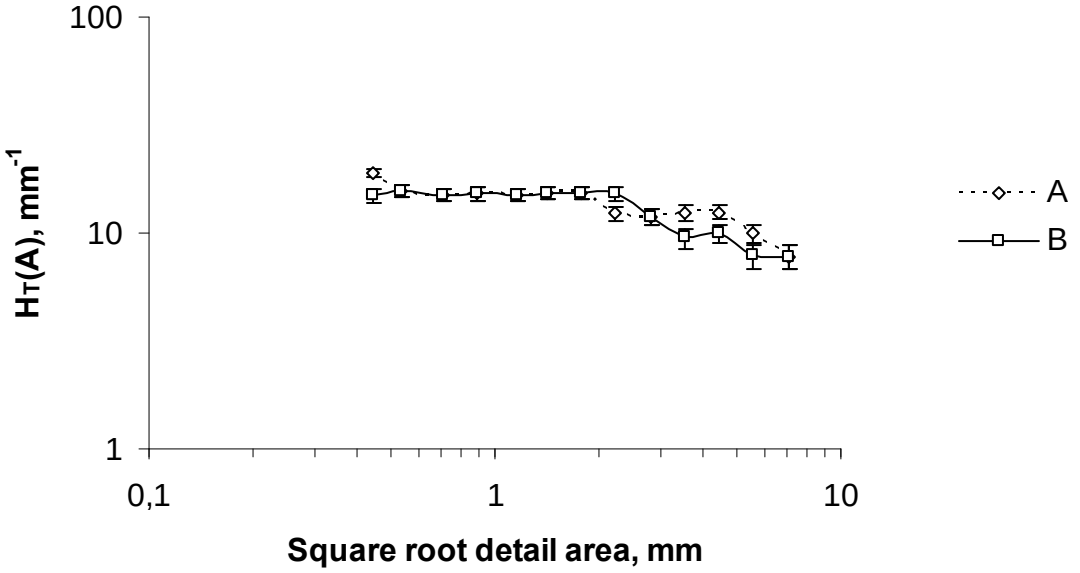

Figure 4.7. Comparison of the threshold contrast-detail index at 125 kV with method based on constant detector entrance dose (A) and method based on constant CNR (B) (15 cm PMMA + CDRAD).

The Figure 4.7. shows that at higher spatial frequencies (i.e. smaller detail objects) absolute value of $H_T(A)$ index for the constant detector entrance dose method compared to the constant CNR methods differs from 26% to 30% and is almost equal at lower spatial frequencies.

Experiments held by Moore and Geijer et al. demonstrate on CDRAD examination analyses that by choosing the appropriate reduction in tube potential, the system can be optimised either for reduction of the effective dose with a constant image quality or for improvement of the image quality at the same effective dose as before optimisation [31, 38]. These changes can easily be implemented in clinical practice. At the same time when AEC is used, in order to keep same TCDD value, ESD needs to be increased when tube potential is reduced; otherwise, the detector entrance dose will be not enough to provide same quality in terms of contrast details (Figure 4.5). The CDRAD phantom evaluates mainly low-contrast objects, which is a limitation. In the same time the visual grading analysis (VGA) used in Geijer study with an anatomical phantom supported the findings [31].

At present study images of an anthropomorphic phantom ("PIXY", Radiology Support Devices (RSD), Long Beach, CA, USA) also were taken to bring a clinical view to the CDRAD phantom physical measurements at different radiation quality ranges. Figure 4.8 shows the chest antero-posterior AP projection images taken at different X-ray tube potentials by using the same setup as for constant detector entrance dose measurements. Because of great effect of post-processing on the image quality the final optimisation must be carried out according to clinical criteria and image post-processing algorithms. However, it is clear, that special contrast-detail physical phantoms (such as CDRAD 2.0) could be much easily be suited for objectivisation and standardisation of image quality constancy tests and optimisation [44, 45].

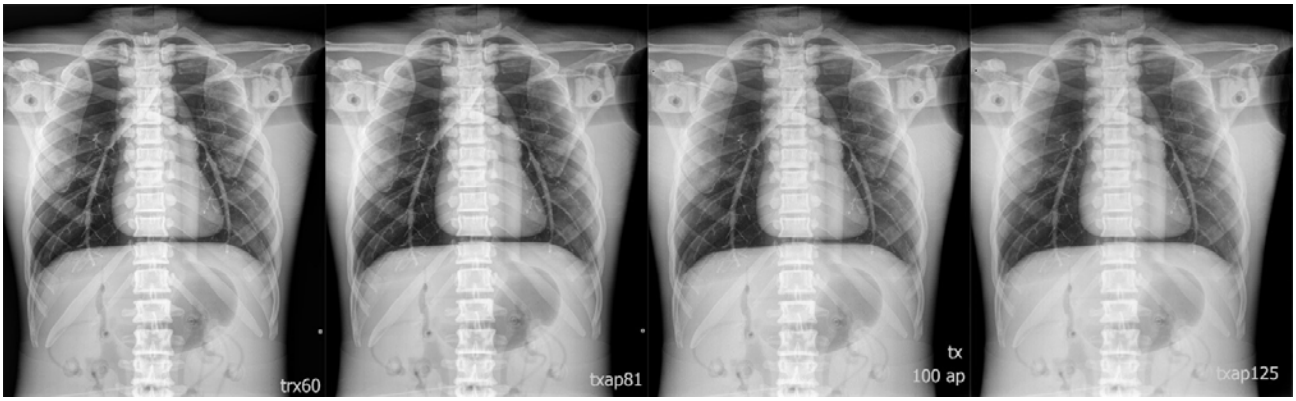

Figure 4.8. The comparison of the image quality using female anthropomorphic phantom at different 60, 81, 100 and 125 kVp with the same detector entrance dose.

4.2. Uncertainty of TCDD measurements

The expanded uncertainties were found for detector dose measurements at 81 kVp, entrance surface dose measurements (ESD) and dose measurements with automatic expose control (AEC).

The statistical uncertainty component for 3,90 μGy of detector dose (D) measurements was $u_A(D)$ = 0,0012 μGy; type B uncertainty was $u_B(D)$= 0,07 μGy; combined standard uncertainty is $u_C(D)$ = 0,07 μGy. The measured detector dose value with expanded uncertainty at 95 % level of confidence (3,90 ± 0,17) μGy.

The statistical uncertainty component for 0,390 mGy of entrance surface dose (D_{ESD}) measurements was $u_A(D_{ESD})$ = 0,00012 mGy, type B uncertainty was $u_B(D_{ESD})$= 0,007 mGy; combined standard uncertainty is $u_C(D_{ESD})$ = 0,007 mGy. The measured ESD value expanded uncertainty at 95 % level of confidence ESD = (0,390 ± 0,016) mGy.

During experiment it was also evaluated statistical component of detector dose (D) when using AEC control. The statistical uncertainty component was $u_A(D)$ = 0,05 μGy. Using AEC instead of manual mode could give rise to additional 1,0% relative uncertainty in detector dose measurements.

For $H_T(A)$ index the maximum measured expanded uncertainty at 95 % level of confidence was 1,2 mm^{-1} which corresponds to relative uncertainty of 7,5 % .

5. CONCLUSIONS

Two methods of automatic exposure control (AEC) setup based on threshold contrast-detail detectability measurements on CDRAD phantom have been examined as a function of X-ray beam quality in a computed radiography (CR) system. It was found that the constant CNR method did not maintain constant $H_T(A)$ index when the X-ray energy has been increased. The constant detector entrance air kerma strategy was more successful at maintaining constant detectability. Deviation between on spatial frequency dependences of the constant CNR method and the constant detector entrance dose method at lower and higher tube potentials was found. It was found that for $H_T(A)$ index the maximum measured expanded uncertainty at 95 % level of confidence was 1,2 mm^{-1} which is lower than average standard deviation of $H_T(A)$ index from reference 81 kVp curve for both constant detector dose and constant CNR methods, which was 1,7 mm^{-1} and 2,4 mm^{-1} correspondently. The results show that TCDD evaluation method is reliable and could be used for the optimisation practice. It was also found that usage of automatic AEC instead of manual setting

could give rise to additional 1% of relative uncertainty in detector dose measurements, which shows that if AEC is used during image quality optimisation the repeatability of AEC control needs to be taken into account, that was absent in the previous studies [41]. However the idea to keep constant contrast–to-noise ratio for every patient independently from tube potential is good, the physical parameter of CNR itself does not give information on the perceptibility of details with different size. Following the Marshall method [4] the detector entrance dose would decrease at lower tube potentials, but the threshold-contrast detail detectability would also drop down up to 63 %. For CR system optimisation the Marshall method could be developed if the constant detector dose method is combined with the constant CNR method to achieve the golden mean. For higher tube potentials the constant CNR method could be fully implemented which will slightly decrease the $H_T(A)$ index at higher spatial frequencies, and at the same time ESD will be slightly increased. For lower tube potentials it is suggested not to decrease fully the detector dose in order to keep constant CNR but decrease it up to 30% of $H_T(A)$ index deviation at lower spatial frequencies. It will maintain slightly increased CNR and slightly decreased ESD. Also according to the previous publication the $H_T(A)$ index is more sensitive to dose reduction at lower tube potentials than higher tube potentials [41]. Although the dependence of both CNR and $H_T(A)$ index on tube potential has been examined in this work, the optimum absolute value of detector entrance dose still needs future investigations. It could be also necessary to calculate effective patient doses for optimised AEC curves by using for example PCMCX software [18]. Still the new optimisation methods using objective physical parameters need further justification by the human observer evaluation methods for medical image quality such as ROC or VGA analysis.

REFERENCES

1. Ulst, M.; Aavik, A.; Käpp, R.; Paats, A. (2008). ESTONIA-PACS – integral part of national e-Health Program. Presented at the Baltic Radiology Congress, Tartu, Estonia, 24-25 October 2008.
2. Vano, E.; Fernandez, J.M.; Ten, J.I et al. (2007). Transition from screen-film to digital radiography: evaluation of patient radiation doses at projection radiography. *Radiology*, 243, 461-466
3. Commission of the European Communities (CEC). (1997). Council Directive 97/43/Euratom of 30 June 1997 on health protection of individuals against the dangers of ionizing radiation in relation to medical exposure, and repealing Directive 84/466/Euratom. *Official Journal of the European Communities,* L 180, 22-27
4. Marshall, N. W. (2009). An examination of automatic exposure control regimes for two digital radiography systems. *Physics in Medicine and Biology*, 54, 4645-4670
5. Honey, I.D.; MacKenzie, A. (2005). Investigation of optimum energies for chest imaging using film–screen and computed radiography. *The British Journal of radiology*, 78, 422-427
6. Schaefer-Prokop, C.M.; De Boo, D.W.; Uffmann, M. (2009). DR and CR: Recent advances in technology. *European Journal of Radiology*, 72, 194-201
7. Lanca, L.; Silva, A.; (2009). Digital radiography detectors – A technical overview: Part 1. *Radiography*, 15, 58-62
8. Sonoda, M.; Takano, M.; Miyamaha, J.; Kato, H. (1983). Computed radiography utilizing scanned laser stimulated luminescence. *Radiology*, 148, 833-838
9. Kotter, E.; Langer, M.; (2002). Digital radiography with large-area flat-panel detectors. *European Radiology*, 12, 2562-70.
10. NHS Purchasing and Supply Agency. (2006). Computed Radiography (CR) Systems for General Radiography, A Comparative Report, Edition 3, *Report 06033*
11. Commission of European Communities (CEC). (2010). Criteria for acceptability of radiological, nuclear medicine and radiotherapy installations. *Final Draft Amended –V1.4-091001 RP91*. Luxemburg: EC, 2010

12. Institute of Physics and Engineering in Medicine (IPEM). (2005). *Recommended standards for the routine performance testing of diagnostic X-ray imaging systems. IPEM Report No. 91*. York (UK): IPEM, 2005.

13. American Association of Physicists in Medicine (AAPM). (2006). *Acceptance Testing and Quality Control of Photostimulable Storage Phosphor Imaging Systems*. AAPM Report No. 93, Task Group 10

14. International Commission on Radiation Units and Measurements (ICRU). (1996). *Medical imaging – the assessment of image quality. ICRU Report 54.* Bethesda, MD: ICRU, 1996

15. International Commission on Radiation Units and Measurements (ICRU). (2003). *Image Quality In Chest Radiography. ICRU Report 70.* Journal of the ICRU Vol.3 No 2, Nuclear Technology Publishing 2003.

16. Smans, K.; Vandenbroucke, D.; Pauwels, H.; Bosmans, H. (2010). Validation an image simulation technique for two computed radiography systems: An application to neonatal imaging. *Medical Physics*, 37, 2092-2100

17. Uffmann, M.; Schaefer-Prokop, C.; (2009). Digital radiography: The balance between image quality and required radiation dose. *European Journal of Radiology*, 72, 202-208

18. Tapiovaara, M.; Siiskonen, T.; (2008). PCXMC, A Monte Carlo program for calculating patient doses in medical x-ray examinations. 2nd Ed. STUK-A231. Helsinki: Radiation and Nuclear Safety Authority.

19. Sandborg, M.; Tingberg, A.; Ulman, G. (2006). Comparison of clinical and physical measures of image quality in chest and pelvis computed radiography at different tube voltages. *Medical Physics*, 33 (11), 4169-4174

20. Pascoal, A.; Lawinski, C.P.; Honey, I.; Blake, P. (2006). Evaluation of a software package for automated quality assessment of contrast detail images – comparison with subjective visual assessment. *Physics in Medicine and Biology*, 50, 5743-5757

21. Doyle, P.; Martin, C.J. and Gentle, D. (2005). Dose-image quality optimisation in digital chest radiography. *Radiation Protection Dosimetry*, 114, 269-272

22. Bourne, R. (2010). *Fundamentals of Digital Imaging in Medicine*. Springler-Verlag London Limited, 2010

23. Fornasini, P. (2008). *The Uncertainty in Physical Measurements: An Introduction to Data Analysis in the Physics Laboratory.* Springer Science, 2008.

24. Bushberg, J.T.; Seibert, J.A.; Leidholdt, E.M, Jr.; Boone, J.M. (2002). *The essential physics of medical imaging*. Philadelphia [etc.]: Lippincott Williams & Wilkins, 2002
25. Tapiovaara, M. (2006). *Relationships between physical measurements and user evaluation of image quality in medical radiology –a review*. STUK-A219. Helsinki: STUK, 2006.
26. Doyle, P.; Gentle, D.; Martin, C.J. (2005). Optimising Automatic Exposure Control in Computed Radiography and the impact on patient dose. *Radiation Protection Dosimetry,* 114, 236-239
27. Veldkamp, W.; Kroft, L.; Geleijns, J. (2009). Dose and perceived image quality in chest radiography. *European Journal of Radiology*, 72, 209-217
28. Rose, A. (1948). The sensitivity performance of the human eye on an absolute scale. *Journal of the Optical Society of America*, 38, 196-208
29. Båth, M. (2010). Evaluating imaging systems: practical applications. *Radiation Protection Dosimetry*, 139, 26-36
30. Dobbins, J.; Samei, E.; Ranger, N; (2006). Intercomparison of methods for image quality characterization. II Noise power spectrum. *Medical Physics*, 33, 1466-1475
31. Geijer, H.; Norrman, E.; Persliden, J. (2009). Optimizing the tube potential for lumbar spine radiography with a flat-panel digital detector. *The British Journal of Radiology*, 82, 62-68
32. Doyle, P.; Martin, C.J. (2006). Calibrating automatic exposure control devices for digital radiography. *Physics in Medicine and Biology*, 51, 5475-5485
33. Zamenhof, R. G. (1982). The optimisation of signal detectability in digital fluoroscopy *Medical Physics*, 9, 688–94
34. Samei, E.; Flynn M.J. (2002). An experimental comparison of detector performance for computed radiography systems. *Medical Physics*, 29, 447–59
35. Doyle, P.; Martin, C J.; Gentle, D. (2006). Application of contrast-to-noise ratio in optimizing beam quality for digital chest radiography : comparison of experimental measurements and theoretical simulations. *Physics in Medicine and Biology*, 51, 2953-2970
36. Commission of European Communities (CEC). (2006). *European guidelines for quality assurance in breast cancer screening and diagnosis*, Fourth edition, Luxemburg, 2006
37. Rampado, O.; Isoardi, P.; Ropolo, R. (2006). Quantitative assessment of computed radiography quality control parameters. *Physics in Medicine and Biology*, 51, 1577-1593
38. Moore, C.S.; Beavis, A.W.; Saunderson, J.R. (2008). Investigation of optimum X-ray beam tube voltage and filtration for chest radiography with a computed radiography system. *The British Journal of Radiology*, 81, 771-777

39. Gallacher, D.J.; MacKenzie, A; Batchelor, S; Lynch, J. and Saunders, J.E. (2003). Use of a quality index in threshold contrast detail detection measurements in television fluoroscopy. *The British Journal of Radiology*, 76, 464-472
40. Artinis Medical Systems. (2006). CDRAD *Analyser –manual. Version 1.1*, March 2006. Zetten (The Netherland): Artinis, 2006. http://www.artinis.com
41. Kepler, K.; Vladimirov, A. (2006). Optimisation strategies introduced for CR at health care centres in Estonia. *Radiation Protection Dosimetry*, 129, 127-131.
42. Cranley, K.; Gilmore, B. J.; Fogarty, G. W. A. and Desponds, L. (1997). *Catalogue of diagnostic X-ray spectra and other data*. *IPEM Report 78*. [CD-ROM]. York (UK): Institute of Physics and Engineering in Medicine (IPEM), 1997.
43. Kepler, K.; Vladimirov, A. (2006). Optimisation of patient doses in digital radiology and the SENTINEL project. In: *Medical Physics in the Baltic States*. Kaunas: Kaunas Technologija, 2006, 69 - 71.
44. Busch, H. P. (2004). *Image quality and dose management for digital radiography. DIMOND III Final Report.* Trier (Germany): Brüderkrankenhaus, 2004.
45. Moore, C.S.; Liney, G.P.; Beavis, A.W. (2007). A method to optimize the processing algorithm of a computed radiography system for chest radiography. *The British Journal of Radiology*, 80, 724-730

SUMMARY

Nowadays radiation dose and image quality optimisation is one of the major tasks of quality assurance in medical digital imaging. Because of broad dynamic range of the computed radiography (CR) systems an inappropriate technique could lead to unnecessary high exposure and potential harm of radiation dose to the patient while keeping a perfect image quality. Therefore there is a need to find out the reliable image quality parameters and optimisation methods which could guarantee an acceptable level of diagnostic performance of the images and at the same could be easily implemented in clinical environment. In the present work the threshold contrast-detail detectability (TCDD) estimated with a CDRAD test phantom by using $H_T(A)$ index at different tube potentials, with keeping constant detector entrance dose, phantom entrance surface dose (ESD) and time-current product (MAS) which correspond to different strategies in dose-quality optimisation practice. It was found that for $H_T(A)$ index the maximum measured expanded uncertainty at 95 % level of confidence was 1,2 mm^{-1} which corresponds to relative uncertainty of 7,5 % and lower than average standard deviation of $H_T(A)$ index from reference 81 kVp curve for both constant detector dose and constant CNR methods. During the experiments also statistical component of image receptor dose was evaluated when using AEC. Using AEC instead of manual mode could give rise to additional 1% of relative uncertainty in detector dose measurements. For the first time the ideal $H_T(A)$ curve was also presented to demonstrate the best theoretically possible threshold contrast-detail detectability. For constant CNR method the average deviation of $H_T(A)$ index for 60 kVp, 100 kVp and 125 kVp from reference 81 kVp curve is 2,4 mm^{-1} which is 41% more than in case of constant detector dose method. In the same time the average absolute value of $H_T(A)$ index is about 10% more than the corresponding value for the constant detector dose method. Also deviation between on spatial frequency dependences of the constant CNR method and the constant detector entrance dose method at lower and higher tube potentials was found. The results of this work could be used for future research and development of constant CNR based method by combining it with the method of constant detector dose, enabling improvement of TCDD at lower tube potentials.

ACKNOWLEDGEMENTS

I would like to thank my supervisor Dr. Kalle Kepler. His scientific experience and clear thinking have many times helped me to find out right direction in labyrinths of different ideas. I also wish to thank my opponent, Professor Antti Servomaa for pre-reviewing the thesis and valuable constructive remarks.

SUMMARY IN ESTONIAN

Pildi kvaliteedi hindamismeetodite võrdlus kompuuterradiograafias

Tänapäeva meditsiinilise digitaal-tehnoloogia kvaliteeditagamise üks peamisi ülesandeid on patsiendidoosi ja pildi kvaliteedi optimeerimine. Kuna kompuuterradiograafia süsteemidele on omane lai dünaamiline diapasoon, võib sobimatu tehnika kasutamine põhjustada suuri kiirgusdoose ja potentsiaalset ohtu patsiendile, kuigi pildi kvaliteet võib jääda samal ajal ideaalseks. Seetõttu on vaja välja selgitada usaldusväärsed pildi kvaliteedi parameetreid ja optimeerimismeetodid, mis suudaksid tagada vastuvõetaval kiirgusdoosi tasemel diagnostilise pildi piisava kvaliteedi ja samal ajal oleksid kergesti kasutatavad kliinilises keskkonnas. Käesolevas töös mõõdeti pildi kvaliteeti iseloomustava parameetrina lävikontrastsus-teravust (TCDD) CDRAD testfantoomiga röntgentoru erinevate pingete korral. Vastavalt pildi kvaliteedi optimeerimise erinevatele strateegiatele katsetati erinevaid meetodeid: detektori konstantse sisenddoosiga, fantoomi konstantse sisenddoosiga (ESD) ning konstantse röntgentoru laenguga (MAS). Leiti, et $H_T(A)$ indeksi maksimaalne laiendmääramatus usaldusväärsusega 95% oli 1,2 mm^{-1}, mis vastab suhtelisele mõõtemääramatusele 7,5%, ja on väiksem kui $H_T(A)$ indeksi keskmine standarthälve kontrollkõvera väärtus (pingel 81 kVp) mõlema meetodi, konstantse CNR ning detektori konstantse sisenddoosi meetodi, puhul. Katsetes hinnati ka detektori sisenddoosi statistilist korduvust automaateksposits ioonisüsteemi (AEC) kasutamisel. Leiti, et kui kasutada AEC-režiimi käsitsirežiimi asemel, kasvas detektori sisenddoosi suhteline mõõtemääramatus kuni 1%. Esmakordselt on arvutatud ja esitatud lävikontrastsuse-teravuse ideaalne kõver, et näidata võrdlusena parimat teoreetiliselt võimalikku $H_T(A)$ indeksi väärtust. Konstantse CNR meetodi puhul oli $H_T(A)$ indeksi kontrollkõvera väärtuse (pingel 81 kVp) ja võrdluskõverate väärtuste (pingetel 60 kVp, 100 kVp ja 125 kVp) vaheline keskmine standardhälve 2,4 mm^{-1}, mis on 41% suurem võrreldes detektori konstantse sisenddoosi meetodiga. Samal ajal oli $H_T(A)$ indeksi keskmine absoluutväärtus ligi 10% suurem vastavast väärtusest detektori konstantse sisenddoosiga meetodi puhul. Samuti leiti, et võrreldud meetodite puhul on $H_T(A)$ sagedussõltuvus erinev madalatel ja kõrgetel röntgentoru pingetel. Käesoleva töö tulemused ja järeldused võivad anda väärtuslikku informatsiooni edasisteks uuringuteks ja konstantse CNR meetodi arendamiseks, kombineerides seda detektori konstantse sisenddoosi meetodiga, võimaldades nii pildi kvaliteedi paremat optimeerimist ka röntgentoru madalate pingete puhul.